

26 May 2010, 4:45 pm - 6:45 pm

# P-Wave Reflection Imaging of Laboratory Soil Models

Joseph Coe
*University of California, Los Angeles, CA*

Scott J. Brandenberg
*University of California, Los Angeles, CA*

Fifth International Conference on
Recent Advances in Geotechnical Earthquake Engineering and Soil Dynamics
*and Symposium in Honor of Professor I.M. Idriss*
May 24-29, 2010 • San Diego, California

# P-WAVE REFLECTION IMAGING OF LABORATORY SOIL MODELS

**Joseph Coe, B.S., M.S.**
Dept. of Civil and Environ. Eng.
University of California
Los Angeles, CA 90095-1593

**Scott J. Brandenberg**
Dept. of Civil and Environ. Eng.
University of California
Los Angeles, CA 90095-1593

ABSTRACT

An ultrasonic p-wave reflection imaging system is used to non-invasively image submerged soil models with embedded anomalies and complex geometric layer contacts. The ultrasonic transducers emit compressive waves into water that subsequently transmit into the underlying soil, and measurements of the reflections are used to construct the images. Properties of the transducers and data acquisition hardware and software are explained. A soil model consisting of embedded high- and low-impedance anomalies, dipping soil layer contacts, and an undulating concrete base layer was imaged using 500 kHz transducers. The geometric features of the model are clearly visible in the images.

## INTRODUCTION

Inadequate knowledge about the subsurface is among the biggest problems in geotechnical engineering. Current standard of practice site investigation techniques leave us with an incomplete understanding of site conditions that is often inadequate to reliably perform engineering predictions (Terzaghi 1947). Uncertainty about subsurface properties also exits in small-scale soil test models such as those created for testing on geotechnical centrifuges. Both initial and final geometries of the centrifuge model are often well characterized by taking hand measurements of the model domain. However, centrifuge models are often subjected to a sequence of loading conditions (e.g. a series of simulated earthquake ground motions) as part of testing. Monitoring the response of the model and its geometry during testing would prove extremely valuable, but currently the lack of tools to perform this task prevents proper implementation.

Medicine faced a similar challenge in the first half of the 20th century, wherein the properties of the inside of the human body could only be observed invasively. This problem lead to the development of non-invasive medical imaging techniques such as ultrasonic p-wave imaging. P-wave reflection imaging has also been often utilized by seismologists to image geologic structures sometimes kilometers below the earth's surface, and has proven useful for locating faults or geologic features that contain oil (e.g., Yilmaz 1987). Both medical ultrasound and seismic reflection imaging rely on the same underlying principle: compressive waves reflecting from anomalies can be recorded and utilized to non-invasively construct an image.

P-wave reflection imaging has seen only limited application at the scale of a typical geotechnical project or model despite its prevalence in other fields and its tremendous potential as a geotechnical investigative tool. A handful of studies have been conducted to demonstrate the potential of p-wave reflection imaging. For example, Lee and Santamarina (2005) conducted a small-scale laboratory test program that utilized 500 kHz ultrasonic transducers to image soil layers, embedded objects, and slurry surface position during sedimentation. Grandjean (2006) utilized a seismic "multi-approach" that identified contaminants in the field using a number of different types of waves, including p-waves (Rayleigh waves and shear were also utilized). Kase and Ross (2004) used reflection imaging in advance of tunnel excavation to identify potentially difficult soil conditions. Nichols et al. (1987) located rebound fracture zones in Pierre shale using shallow seismic reflection imaging. More work is necessary to adapt sensors and data processing methods for p-wave reflection imaging at the geotechnical scales of interest.

This paper utilized ultrasonic transducers to image a soil model similar in scale to those often tested in large geotechnical centrifuges. The properties of the transducers and data

acquisition system are presented first, followed by a study of a soil model with a geometry that was made deliberately complex to test the limits of the imaging system. The resolution of the system is tested by comparing the migrated image of the undulating concrete base layer with hand measurements of its surface topography.

## SYSTEM COMPONENTS

The system components for these experiments are the ultrasonic transducers, source pulser, receiver amplifier, receiver analog filter, string potentiometer, terminal block (SCC-68), data acquisition cards mounted in a PXI chassis, and a personal computer (Fig. 1). Many of the components were designed for implementation on the *nees@UCDavis* geotechnical centrifuge, and were initially tested at Georgia Tech by Lee and Santamarina (2005). A steel housing contained the transducers, pulser, amplifier and filter, (together, these components are hereafter called the ultrasound device) and was attached to a frame that held the tips of the transducers in contact with water, and permitted the ultrasound device to smoothly glide horizontally.

### Ultrasonic Transducers

The properties of the ultrasonic transducers are summarized in Table 1, and were first described by Lee and Santamarina (2005). The transducers are composed of a piezoelectric disc -shaped element, backing block, matching layer, and an insulating casing. Imposing a voltage across the source piezoelectric element causes it to rapidly vibrate and induce a compressive wave in the media to which it is coupled. The reflected wave energy distorts the piezoelectric material in the receiver transducer and produces a measureable voltage potential across the element. The nominal frequency of the transducer is controlled by the thickness and stiffness of the disc. The pulse duration is controlled by the backing block, which effectively acts as a damper by absorbing some of the energy radiating from the piezoelectric disc. Short pulse durations (from highly damped transducers) are desired for imaging applications because "spiky" signals provide better image quality than "ringy" signals. However, damping decreases signal amplitude which limits penetration depth of the ultrasonic waves. The matching layer optimizes the wave energy

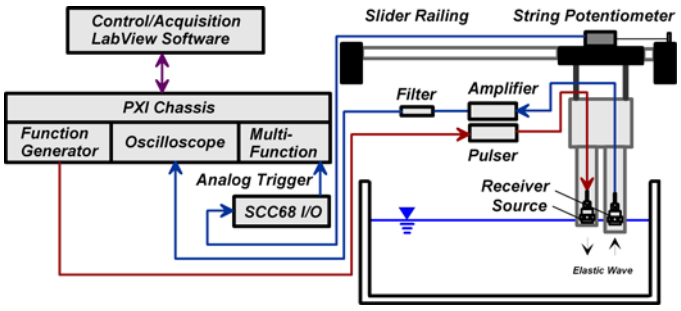


*Figure 1: System components.*

that is transmitted from the transducer, and is configured to favor the transducer's central frequency thereby acting as a band-pass filter. The impedance of the matching layer is typically selected to be the geometric mean of the impedance of the piezoelectric element and the material in contact with the matching layer to maximize energy transmitted from the transducer (i.e. impedance matching). The casing electrically grounds the transducer and provides a mechanical shield that prevents direct arrival of compressive waves from source to receiver.

Table 1. Transducer Properties

| Property | Value |
|---|---|
| | |
| Nominal Frequency | 500 kHz |
| Manufacturer | Panametrics |
| Product No. | A3441 |
| Length | 32 mm |
| Diameter | 19 mm |

### Source Pulser

A custom pulser provided a 150 VDC input signal to the source transducer (Table 2). A high voltage pulse was desired to maximize the pulse amplitude to improve penetration depth and signal-to-noise ratio. The pulser receives +5 VDC power, and is triggered by a 0 to +5 VDC step function from an arbitrary waveform generator. The pulser outputs a step function to the transducer, which subsequently responds predominantly at its central frequency. A step wave duration equal to half of the natural period of the transducer was found to optimize the output signal amplitude.

Table 2. Pulser Properties

| Property | Value |
|---|---|
| | |
| Manufacturer | JSR Ultrasonics |
| Product No. | PCU-QP3 PCU0021 |
| Input Power | 5V DC |
| Output Voltage | 150V DC |
| Input Function | 0 to 5V DC Amplitude Step |

### Receiver Amplifier & Filter

An inline amplifier and analog filter were utilized to record the voltage signal from the receiver transducer (Table 3). The amplifier was located near the receiver transducer in the casing to minimize cable length for the unamplified signal thereby reducing noise and minimizing loss of charge in the cable from the capacitive transducer. The amplified signal was subsequently filtered using a low-pass anti-aliasing filter with corner frequency of 2.5 MHz.

Table 3. Receiver Filter & Amplifier Properties

| Property | Value | Value |
|---|---|---|
| | | |
| Component | Amplifier | Filter |
| Manufacturer | Mini-Circuits | Mini-Circuits |
| Product No. | ZFL-500LN | BLP-1.9 |
| Input Power | 15V DC | N/A |
| Pass Band | 0.1 to 500 MHz | N/A |
| Corner Frequency | N/A | 2.5 MHz |
| Gain | 24 dB Min | N/A |

String Potentiometer

A linear string potentiometer (Table 4) measured the horizontal position of the transducers, and was used to trigger pulses at specified positions as the ultrasonic device was slid by hand on a rail from one end of the model to the other. Triggering intervals as small as 1mm were utilized successfully using the string potentiometer. The automated triggering mechanism facilitated rapid acquisition of hundreds of pulses in only a few seconds, compared with hours that would have been necessary to manually advance the transducers and stop each time an acquisition was desired.

Table 4. String Potentiometer Properties

| Property | Value |
|---|---|
| | |
| Manufacturer | Unimeasure, Inc. |
| Product No. | LX-PA-25 |
| Input Power | 15V DC |
| Range | 625 mm (25 in) |
| Linearity | ± 0.5% |
| Sensitivity | 1.546 mV/V/mm |

Computer Hardware & Software

Data acquisition was controlled by National Instruments cards mounted in a PXIe chassis (NI PXIe-1062Q) connected to a personal computer running LabView software. The pulser was triggered by an arbitrary waveform generator card (NI PXI-5412), and the receiver was sampled at 5 MHz by a high speed digitizer card (NI PXI-5620). The string potentiometer was connected to a NI SCC-68 terminal block expansion slot and sampled using a multi-function card (NI PXI-6259). These three cards were synchronized through the internal clock of the PXIe chassis.

Custom Labview software was written to trigger the ultrasonic device based on readings from the string potentiometer. A single recorded pulse for the 500 kHz transducers exhibited low signal-to-noise ratio, so fast stacking (Brandenberg et al. 2008) utilized a rapid succession of 5000 pulses to improve signal quality. The rapid succession of pulses was subsequently averaged to attenuate noise (presumably random) but not the desired portion of the signal which was well-correlated among the 5000 pulses. Only the resulting averaged pulse was written to file at each specified trigger point. The additional time required to perform fast stacking compared with the time required to send a single pulse did not affect the rate at which the device could be advanced along the length of the model (at an approximate rate of about 15 mm/s). Metadata containing the sampling frequency, trigger points, and other salient information was written as a header above the recorded voltage vectors.

SOIL MODEL IMAGING

Figure 2 illustrates the 3-dimensional soil model used in this study, which was constructed to observe the ability of the system to image objects with irregular surfaces, dipping soil layer contacts, and to measure spatial resolution. Material properties of the model constituents are summarized in Table 5. The internal dimensions of the model were approximately 550 mm in length, 420 mm in width, and 300 mm in depth. Uniform 60-mesh silica sand was air pluviated to form two distinct layers with loose sand over medium dense sand with

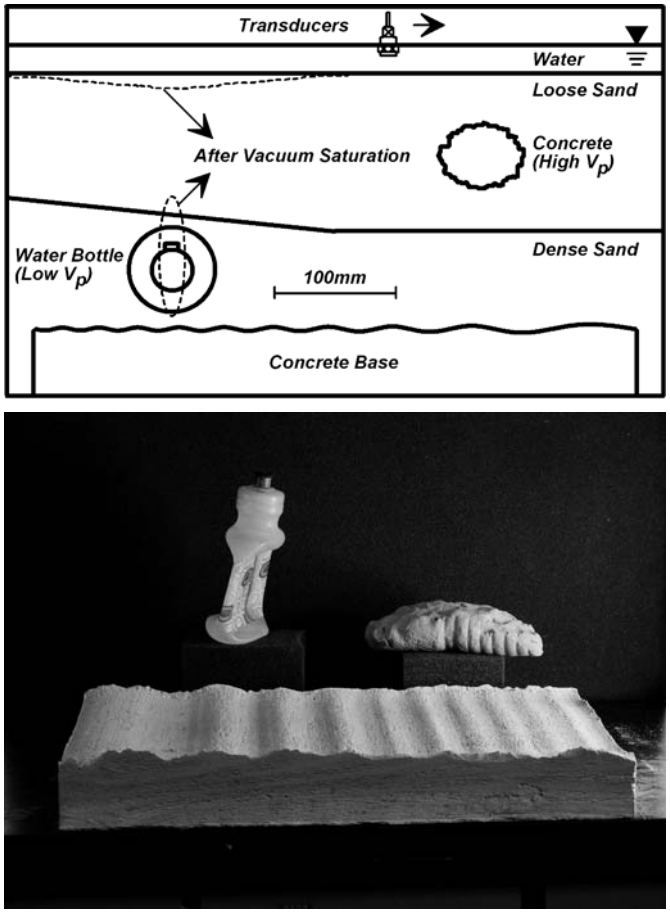


*Figure 2: Model configuration.*

a horizontal contact on the right side of Fig. 2, and a dipping contact on the left side. The difference in densities was achieved by varying drop height. A concrete base with an undulating surface of varying spatial frequency was placed at the bottom of the model to test the resolution of the system, a high-impedance anomaly composed of concrete formed into an irregular cylindrical shape was embedded into the loose sand layer, and a low-impedance anomaly composed of an empty low-density polyethylene (LDPE) water bottle was embedded in the medium-dense sand layer. Properties of the LDPE were based on manufacturer specifications because the wall thickness of the bottle was too small to accurately measure its properties. These embedded objects extended through only half of the width of the model so that the soil layer contacts on the other half could be imaged without embedded anomalies. The model was saturated by placing the inside of the container under vacuum, and subsequently dripping de-aired water through tubes to the bottom of the model. The LDPE water bottle collapsed when the vacuum was released from the container, and its approximate shape and position before and after saturation are shown in Fig. 2. Collapse of the bottle also caused the soil surface to settle.

Table 5. Material Properties

| Property | Dense Sand | Loose Sand | Concrete | LDPE |
|---|---|---|---|---|
| | | | | |
| $G_S$ | 2.67 | 2.67 | - | - |
| $D_{50}$ (mm) | 0.31 | 0.31 | - | - |
| USCS Symbol | SP | SP | - | - |
| e | 0.69 | 0.92 | - | - |
| $\rho$ (kg/m$^3$) | 1990 | 1870 | 2237 | 920 |
| $V_P$ (m/s) | 1556 | 1532 | 2588 | 1950 |
| $Z = \rho_{sat} V_P$ (kg/m$^2$s) | 3.10x10$^6$ | 2.86x10$^6$ | 5.79x10$^6$ | 1.79x10$^6$ |

Ultrasonic images were constructed by gliding the device along the guides and triggering at 5-mm intervals along the length of the model. The voltage values recorded by the receiver transducer were mapped to an 8-bit grayscale image. A Kirchoff migration algorithm was applied to the recorded image to render a more accurate model geometry (e.g., Yilmaz 1987). Figure 3 illustrates the results of overlaying the migrated image of the undulating concrete base layer with measurements taken by hand. The migrated image accurately characterized the geometry of the concrete base layer, particularly for the low-frequency spatial undulations on the right side of the figure. The image on the left side of the migrated section is less clear, though the undulations are evident even for the shortest spatial period of about 40 mm (left side of Fig. 3). In general, the peaks and valleys are clearly evident, while the slopes in between are less clear. This is due to the influence of directivity and the fact that the peaks and valleys act essentially as flat reflectors. Inclined reflectors return less enery due to directivity. A general rule of thumb for locating the depth of a reflector is that transducer resolution is equal to one wavelength, but Fig. 3 indicates that lateral resolution is poorer. The wavelength for the 500 kHz

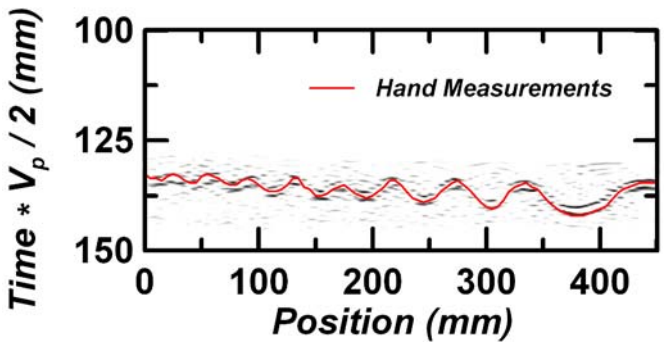


*Figure 3: Ultrasonic image compared with measured position of concrete base layer.*

transducers was approximately 3 mm (wavelength = Vp/f), but the concrete base layer was already becoming unclear at a spatial period of 40 mm. Hence, the rule of thumb that resolution is equal to one wavelength should not be applied for horizontal resolution, and resolution of a testing system should be carefully characterized prior to any experimental study to verify that experimental requirements are met.

A 3-dimensional image of the model was constructed by collecting 2-dimensional scans at 5-mm intervals along the width of the model, forming a 5-mm square grid of measurements in plan view. The voltage values were mapped to 8-bit grayscale voxels (i.e. 3-dimensional pixels) using the software package Voxler (manufactured by Golden Software). The shade of each voxel was proportional to the amplitude of the voltage value from the migrated sections of the records, similar to the 2-dimensional cases already presented. Figure 4 shows several snapshots of the 3-dimensional image from various points of view. All of the major features of the soil model are clearly visible, including the concrete base layer, water bottle, concrete anomaly, and soil layer contact. Shadowing artifacts are apparent on the concrete base and soil layer contacts where the embedded anomalies reflected so much of the energy from the compressive waves that the amplitude of the transmitted waves was too low for imaging purposes. The water bottle was imaged approximately as a line above the loose/dense sand interface, which is consistent with the shape of the collapsed bottle. The bottle also rotated as it collapsed, becoming higher near the center of the model than at the boundary. This information would be difficult to discern from multiple 2-dimensional sections, but is clear in the 3-dimensional image. Finally, Voxler permits the user to rotate the 3-dimensional image to observe it from any desired perspective, and the ability to move the image renders a clarity of the embedded objects that cannot be captured in a still shot (which cannot be demonstrated in this paper).

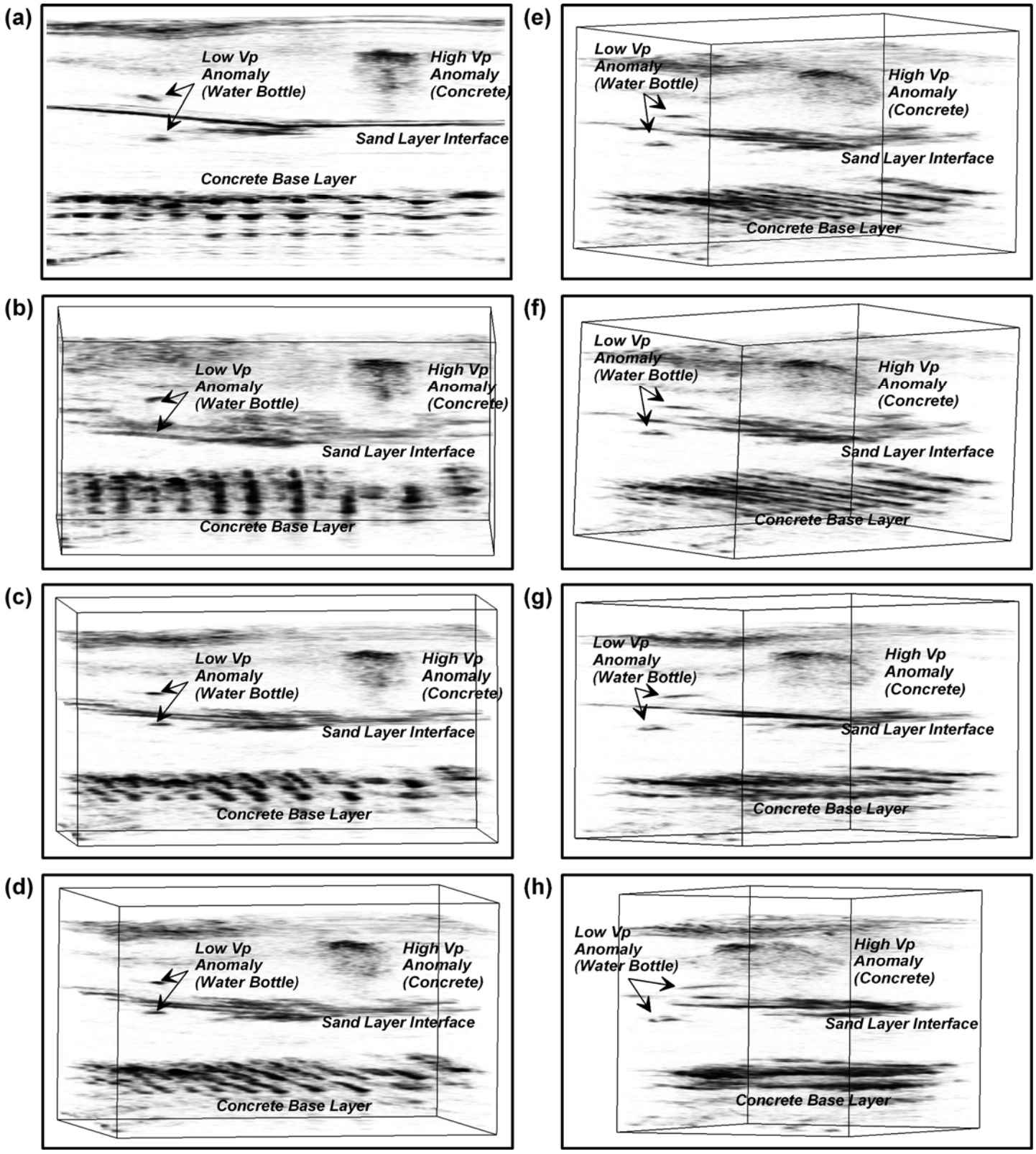


*Figure 4: Three-dimensional ultrasonic image of model from various visual points of view to illustrate model properties.*

## DISCUSSION

Saturation of the sand is crucial for p-wave reflection imaging because unsaturated soil pockets have significantly lower p-wave velocity than saturated soil at the same relative density, and therefore pose an impedance contrast that scatters the seismic waves. In the study presented in this paper, such a high degree of saturation could be obtained by vacuum saturating the models, but not by water pluviation. The surface of the soil was visible in images of the water-pluviated soil, but reflections from the interior of the model were not recorded, presumably because air bubbles scattered the waves. In this regard, the ultrasonic testing system may also prove useful for verifying whether a soil model is adequately saturated. P-waves are often utilized to verify saturation in soil models, and the waves are often generated using p-wave hammers or by striking a plate on the soil surface with a hammer. For example, Naesgaard et al. (2007) generated p-waves with frequency in the range of 3500-7000 Hz in a soil model with air bubbles of controlled size, and found that high p-wave velocities were measured even when Skempton's B-values were low (indicating poor saturation) when the air bubbles were large. They explained that the p-waves may propagate through a saturated soil matrix, bypassing and masking unsaturated pockets. The ultrasonic system presented in this paper would not mask unsaturated pockets, but rather could potentially be used to image the size and position of large air bubbles (at least as small as about 40 mm for the 500 kHz transducers based on Fig. 3).

## CONCLUSIONS

An ultrasonic p-wave reflection imaging system was used to construct images of submerged soil models with embedded anomalies and complex geometric layer contacts. The transducers were held in contact with water above the soil model, and manually slid across the model while p-waves were transmitted and recorded at specified positions. P-wave reflection imaging has significant potential in geotechnical site investigation for imaging laboratory soil models. For example, the geometry of centrifuge models are often measured before and after imposing a sequence of loading events (e.g., earthquake ground motion) on the model, and it is often unclear which loading events caused which fraction of changes in the geometry. The system documented herein provides a method for measuring the geometry in between loading events. More work is required to transition this well-established imaging technique to the geotechnical field and laboratory scale.

## ACKNOWLEGEMENTS

The authors would like to thank Navid Shirazi for helping to characterize the sand properties by various air pluviation techniques. Funding for the project was provided by UCLA, *nees@UCLA,* and Caltrans under contract No. 59A0691.

## REFERENCES

Brandenberg, S.J., Kutter, B.L., and Wilson, D.W. [2008]. "Fast stacking and phase corrections of shear wave signals in a noisy environment." J. Geotech. Geoenviron. Eng., 134(8), pp. 1154-1165.

Grandjean, G. [2006]. "A seismic multi-approach method for characterizing contaminated sites." J. of Applied Geophysics. 58. pp. 87-98.

Gray, S.H., Etgen, J., Dellinger, J., and Whitmore, D. [2001]. "Seismic Migration Problems and Solutions." Geophysics, 66 (5), pp. 1622-1640.

Kase, E.J., and Ross, T.A. [2004]. "Seismic imaging to characterize subsurface ground conditions in civil construction." *Proc. Geo-Trans, 2004.* ASCE Special Publication No. 126. pp. 1823-1831.

Krautkramer, J., and Krautkramer, H., [1990]. "*Ultrasonic testing of materials*." 4th ed. Springer Verlag, Berlin.

Lee, J. S., and Santamarina, J. C. [2005]. "P-Wave Reflection Imaging." Geotech. Test. J., 28(2), pp. 197–206.

Naesgaard, E., Byrne, P.M., and Wijewickreme, D. [2007]. "Is P-wave velocity an indicator of saturation in sand with viscous pore fluid?" Int. J. Geomechanics. 7(6). pp. 437-443.

Nichols, T.C., King, K.W., Collins, D.S., and Williams, R.A. [1987]. "Seismic-reflection technique used to verify shallow rebound fracture zones in the Pierre Shale of South Dakota." Can. Geotech. J. 25, pp. 369-374.

Schneider, W.A. [1978]. "Integral Formulation for Migration in Two and Three Dimensions." Geophysics, 43(1), pp. 49–76.

Stotzka, R., Ruiter, N.V., Mueller, T.O., Rong, L., and Hartmut, G. [2005]. "High resolution image reconstruction in ultrasound computer tomography using deconvolution." *Proc. Medical Imaging 2005: Ultrasonic Imaging and Signal Processing*. W. Walker, S. Emelianov eds. Vol. 5750, pp. 315-325.

Terzaghi, K. [1947] "*Theoretical soil mechanics*." Fourth Printing. John Wiley and Sons, Inc., New York.

Yilmaz, O. [1987]. "*Seismic Data Processing*." Society of Exploration Geophysicists, Tulsa, Oklahoma.